Wind and Structures, *Vol. 31, No. 1 (2020) 43-57*
DOI: https://doi.org/10.12989/was.2020.31.1.43

Effects of wind barriers on running safety of trains for urban rail cable-stayed bridge

Wei He[1,2a], Xiang-Rong Guo[3], Zhi-hui Zhu[3], Pengru Deng[*4] and Xu-hui He[3]

[1]School of Civil Engineering, Anhui Jianzhu University, Hefei, 230601, China
[2]National Engineering Laboratory for Structural Health Monitoring and Disaster Prevention, Anhui Jianzhu University, Hefei, 230601, China
[3]School of Civil Engineering, Central South University, Changsha, 410075, China
[4]Faculty of Engineering, Hokkaido University, Sapporo, 0608628, Japan

(*Received January 7, 2020, Revised May 31, 2020, Accepted July 11, 2020*)

Abstract. Considering the wind barriers induced aerodynamic characteristic variations of both bridge deck and trains, this paper studies the effects of wind barriers on the safety and stability of trains as they run through an urban rail transit cable-stayed bridge which tends to be more vulnerable to wind due to its relatively low stiffness and lightweight. For the bridge equipped with wind barriers of different characteristics, the aerodynamic coefficients of trains and bridge decks are obtained from wind tunnel test firstly. And then, the space vibration equations of the wind-train-bridge system are established using the experimentally obtained aerodynamic coefficients. Through solving the dynamic equations, one can calculate the dynamic responses both the trains and bridge. The results indicate that setting wind barriers can effectively reduce the dynamic responses of both the trains and bridge, even though more wind forces acting on the bridge are caused by wind barriers. In addition, for urban rail transit cable-stayed bridges located in strong wind environment, the wind barriers are recommended to be set with 20% porosity and 2.5 m height according to the calculation results of cases with wind barriers porosity and height varying in two wide ranges, i.e., 10% - 40% and 2.0 m to 4.0 m, respectively.

Keywords: wind barrier; train; cable-stayed bridge; wind tunnel test; coupled vibration

1. Introduction

The crosswind has always been a threat to the running safety of trains, especially for the moving trains on bridges because the altitude-dependent wind velocity at the bridge deck level is normally higher than that at the ground level. Besides, the wind-induced load on the trains is exaggerated due to the train-bridge aerodynamic interaction, which further deteriorates running safety of the trains (Dorigatti *et al*. 2012, Han *et al*. 2014). Dynamic analyses of coupled train and cable-stayed bridge systems under winds indicated that the dynamic responses of trains passing long-span bridges are more sensitive to the wind load than those on other types of bridges due to the relatively low structural rigidity (Xu *et al*. 2003, Xu *et al*. 2004, Xu *et al*. 2004, Li *et al*. 2005). Especially, for a cable-stayed bridge in urban rail transit as in this study, the wind-induced condition may be more serious as the bridge is with a long span and the superstructure is in the form of a steel girder with smaller height and weight than concrete girder. Thus, it is of great significance to improve the running safety of the urban rail transit special cable-stayed bridges located in strong wind environments. Fortunately, the wind barriers afford a possible solution as they can effectively improve the traffic safety by providing a relatively low wind environment for the train (Baltaxe *et al*. 1967, Kwon *et al*. 2011, Chu *et al*. 2013, Santiago *et al*. 2007). However, even though the setting of wind barriers on bridge deck reduces the wind load on the trains, it induces more loads to the bridge and also changes the aerodynamic characteristics of bridge deck (Charuvisit *et al*. 2004, Xiang *et al*. 2018, Zhang *et al*. 2018, Kozmar *et al*. 2012, Buljac *et al*. 2017). According to the existing researches, it was unwise to apply the normally exploited wind barriers to the bridges with very low stiffness. Especially for the urban rail transit special cable-stayed bridge, the stiffness and weight are much smaller than normal urban rail transit bridges. The wind load induced by the wind barriers may cause remarkable deformations and vibrations of the bridge located in a strong wind environment as the small cross section cannot provide enough stiffness to resist the wind forces and the light self-weight of bridge girder cannot provide sufficient restoring forces to reduce the wind-induced deformation rapidly. These deformations and vibrations further affect the running safety of the urban rail transit trains on the bridge. Therefore, it is essential to account for this combined effect of wind barriers and the bridge deck and trains on the aerodynamic characteristics of the corresponding objects.

In this study, wind tunnel tests are conducted on the train-bridge deck system equipped with wind barriers to investigate the performance of the wind barriers. The

*Corresponding author, Ph.D. Assistant Professor
E-mail: pengrudeng@eng.hokudai.ac.jp
[a]Ph.D.
E-mail: hewei@ahjzu.edu.cn

http://www.techno-press.com/journals/was&subpage=7
ISSN: 1226-6116 (Print), 1598-6225 (Online)

performance of the wind barriers includes the influence of wind barrier on the aerodynamic loading of trains and bridge decks. In order to measure the dimensionless force coefficients of both the bridge deck and train in a train-bridge combination state, this study employs a new measuring method, where two pairs of force balances are equipped on the train and bridge deck segment models, respectively. Thus, the aerodynamic forces of bridge and train can be obtained concurrently. In other words, the two forces are measured at the same time. Actually, in previous studies, the method of obtaining aerodynamic forces of the bridge deck and trains is a step-by-step measurement by changing the measuring position of the force balances in a wind tunnel. That is, two force balances are firstly installed at both ends of the train segment model for measuring, and then they are installed at both ends of the bridge segment model (Li *et al*. 2004, Han *et al*. 2013, Guo *et al*. 2015). The dynamic similarity in fluid mechanics is the phenomenon that if two geometrically similar vessels possess the same boundary conditions together with the same Reynolds number, the fluid flows in these vessels can be regarded as identical to each other. Although this method is feasible based on the dynamic similarity in fluid mechanics, the measuring errors which are possibly caused due to changing the position of the force balances are difficult to be avoided. With the new measuring method in this study, these errors can be avoided.

Moreover, using the measured aerodynamic coefficients, this study analyzes the effects of key factors of wind barrier on the aerodynamic characteristics of the bridge deck and trains for the urban rail transit special cable-stayed bridge. According to the findings presented in (Su *et al*. 2017, He *et al*. 2016, Simiu *et al*. 1996, Gandemer 1981, Judd *et al*. 1996), various factors affect the aerodynamic characteristics of the wind barrier. Based on the references, porous barriers have been proved to be more efficient than solid barriers in wind protection (Lee *et al*. 1998), and porosity is identified as one critical parameter determining the performance of the wind barriers (Heisler *et al*. 1988; Lee *et al*. 1999, Kwon *et al*. 2011). Additionally, height is also one key factor affecting the aerodynamic characteristics of wind barriers according to the existing results (Cornelis *et al*. 2005, Chu *et al*. 2013, Kozmar *et al*. 2014). It is generally accepted that the optimum height of the wind barrier needs to consider the height of the vehicles, whereas different vehicles may have very different dimensions. Hence, the conclusions of the previous studies cannot be directly used (Chu *et al*. 2013). In addition, the height and porosity of the wind barrier on bridges need to be adjusted according to the train and bridge type to achieve the best wind protection (Kozmar *et al*. 2014). However, these studies reveal the interdependent between porosity and height of wind barriers on the bridge only from the perspective of aerodynamic analysis. Under the combined action of train-induced load and wind-induced load, the low stiffness and lightweight bridge will produce large deformation and vibration, and this coupled vibration will affect the running safety of the train. Therefore, it is necessary to study wind barrier influence mechanism from the perspective of aerodynamic analysis but also the perspective of wind-train-bridge coupled vibration analysis when the bridge has low stiffness and lightweight. Furthermore, compared with high-speed trains, urban rail transit trains have larger geometric dimensions and a lighter weight, which means more wind forces will be applied on the trains and the restoring force from the self-weight may be insufficient. Thus, more attentions should be paid on the running safety of the urban rail transit trains, especially under a strong crosswind environment. This also indicates that the contributions of the previous studies on wind barrier for high-speed railway bridge are not fully applicable to urban rail transit special cable-stayed bridge. In order to obtain the optimal value of porosity and height of wind barrier on urban rail transit special cable-stayed bridge, the following research is carried out.

Taking the first urban rail transit special cable-stayed steel box girder bridge (Gaojiahuayuan Bridge) of China as the engineering background, this paper studies influence mechanism of wind barrier on urban rail transit trains running safety not only from the perspective of aerodynamic analysis but also from the perspective of wind-train-bridge coupled vibration analysis. Hence, the research is completed in two steps. In the first step, the aerodynamic coefficients of the trains and the bridge beams are obtained from wind tunnel experiments on the bridge beams equipped with wind barriers of various porosities and heights. The second step is to establish and solve the coupled vibration equation of the train-bridge system subjected to fluctuating wind loads. In this step, a modified spectral representation method is used to generate the spanwise stochastic wind field, and then the aerodynamic coefficient obtained in the first step is adopted to realize the simulation of the wind-induced load of the train-bridge system. The coupled vibration equation of the train-bridge system subjected to wind-induced load is established to study the influence mechanism of wind barrier factors on the running safety of urban rail transit cable-stayed bridge. Moreover, using the established coupled vibration model, the relation between the characteristics of wind barriers including the porosity and height and the dynamic responses of bridge and trains including acceleration histories, rate of wheel load reduction and derailment coefficients are obtained as the trains run through the urban rail transit cable-stayed bridge with different speeds and under different wind speeds environments. With these relations, one can have a clear image of the effects of setting wind barriers on the running safety and urban rail trains on the cable-stayed bridge. Additionally, these relations can provide references for the wind barrier setting on the other urban rail transit cable-stayed bridge. Furthermore, to facilitate application, a recommendation on the parameter values of the wind barriers is suggested for this bridge under strong wind conditions.

2. Wind tunnel tests

The wind tunnel tests in this paper are carried out in the high-speed railway wind tunnel at Central South University. It is a closed-circuit atmospheric boundary layer wind

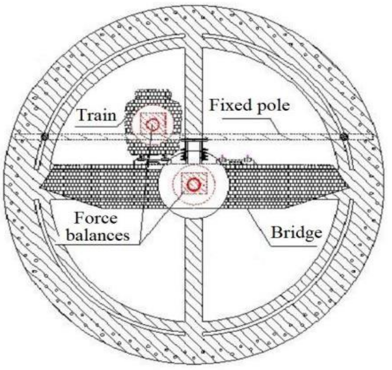

Fig. 1 Schematic diagram of measuring equipment in wind tunnel

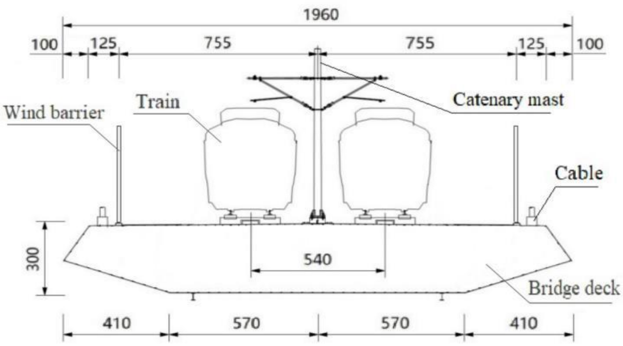

Fig. 2 Cross-section of bridge deck (unit: cm, full-scale)

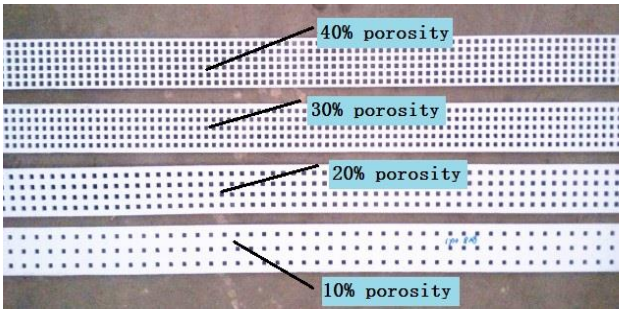

Fig. 3 Photograph of 1/40 scaled model of wind barriers

(a) The front view

(b) The side view

Fig. 4 Photograph of aerodynamic force testing device of train-bridge system

tunnel with two test sections: the low- and high-speed sections. In order to reduce the effects of turbulence and obtain the aerodynamic forces more accurately, the section model is tested in the high-speed section of the wind tunnel which can provide a low turbulence level. For the wind tunnel test of bridge, dynamic similarity exists when the model and the prototype have the same length scale ratio. The train and bridge girder (including the wind barrier) are modeled as rigid bodies with a geometrical scale of 1: 40 in the wind tunnel tests to obtain aerodynamic forces of train and bridge. However, due to failure to achieve Reynolds number similarity, Reynolds number effects in the flow around a bluff and sharp edged bridge girder cross section exist in the most wind tunnel test of scale model (Schewe *et al*. 1998). Although it is impossible to achieve the same Reynolds number in the model and the prototype, one can reduce Reynolds number effects. One common approach is designing the wind tunnel test to have a Reynolds number falling in a range which makes the Reynolds number effect not obvious. As reported in wind tunnel tests (Larsen *et al*. 1998, Matsuda *et al*. 2001, Guo *et al*. 2015), 10^4 to 10^6 could be an appropriate and acceptable range for aerodynamic force measurement of bridge girders. Wind tunnel tests considered the combined effects of wind barriers on the aerodynamic characteristics of the bridge deck and trains. Measured with four force balances, the aerodynamic forces of trains and bridge decks were obtained in the train-bridge combination state concurrently as shown in Fig. 1. Compared to previous measurements with two force balances, the measurement error caused by changing the position of the force balances can be avoided in this study. The four force balances were mounted on both ends of the train and bridge deck section models.

2.1 Test model

The tested section model includes the bridge deck section model, the train section model, and the detachable wind barrier model. The train section model is based on the A-type rail transit passenger train (GB50157-2013), which is currently used in most urban rail transit transits in China. The size of the cross-section of the A-type rail transit passenger train is 3.38 m wide, and 3.50 m high, which is much larger than the size of the cross-section of the high-speed train. Thiscauses the A-type rail transit passenger train's body to be subjected to greater lateral wind-induced load in the crosswind. The bridge deck section model is based on the bridge deck of Gaojiahuayuan Bridge. As there are only two lanes on this urban rail transit special bridge deck, the size of the cross-section of the bridge deck which is 19.60 m wide and 3.00 m high is much smaller than the road-rail bridge deck. Fig. 2 shows the cross-section of the bridge deck. As the catenary mast can hardly affect the aerodynamic characteristics of the train and bridge, it is not included in the test section model. For the 3.50 m height of the urban train, 2.5 m, 3.0 m, 3.5 m, 4.0 m are selected as the height of the wind barriers. Moreover, 10%, 20%, 30%, 40% are selected as the porosity of the wind barriers and the wind barrier model is scaled down on these bases.

In the current wind tunnel experiment, the scale ratio between the test model and the real structure was chosen to be 1:40 for all tested models. Accordingly, the dimensions of the train model are 2000 mm long, 110 mm high and 89 mm wide, and the length (L), height (H), and width (W) of the bridge deck model are 2000 mm, 75 mm, and 490 mm, respectively. On both sides of the bridge deck, wind barrier models with different porosities and heights are set up at a distance of 189 mm away from the centreline of the bridge deck. According to previous researches, it is well known that the pore size and form of the wind barrier can affect the performance of the wind barrier (Dong *et al*. 2007, Xiang *et al*. 2014, Xiang *et al*. 2015). In order to make all the results comparable, all wind barriers are equipped with the same pore size and form which adopts evenly distributed rectangular holes of dimensions 8×8 mm in this experiment as shown in Fig. 3. All of these wind barrier models are detachable, so in each test case, only the wind barrier models need to be changed, while the train and bridge deck model and the force balances are maintained as they are.

2.2 Test conditions and data processing

All test cases were conducted with a uniform oncoming flow in the high-speed test section. The oncoming flow velocity U is 10 m/s, corresponding to a Reynolds number of 1.23×10^5 based on U and H (the height of the train-bridge system model). The wind barrier models were installed on the bridge deck model, and the train model and the bridge deck model were separated. Fig. 4 shows the photo of the experimental setup for this wind tunnel test. To measure the aerodynamic forces on the train model and the bridge deck model, a couple of force six-component balances (NITTA, Inc., Jap.) was set on the two ends of either the train model or the bridge model in the flow. Hence, the aerodynamic forces acting on both models can be measured separately but simultaneously accounting for the influences due to the existence of each other. With four force balances, the measurement method in this study can avoid the measurement error caused by changing the position of the force balances. At each end of the segment model, six components including the three forces (lift, drag, and side) and the three moments (pitch, roll, and yaw) can be measured with the balance. The measurement ranges of each component sensor are lift force and drag force: ±100N, side force: ±200N, moments of pitch, roll, and yaw: ±11N·m. As the geometry scale of the segment model and the wind speed scale are selected to be 1/40 and 1/2

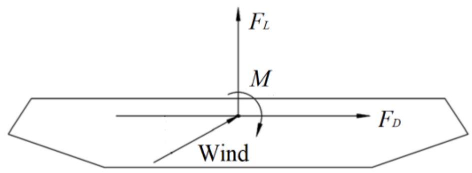

Fig. 5 Diagram of the body axis system

respectively, the sampling duration is chosen20 swith respect to the duration of crossing the prototype bridge of 40s (Yoshie *et al*. 1997). On the basis of the measured data, the aerodynamic coefficients of the bridge and the train were calculated respectively.

$$C_D = \frac{F_D}{1/2\rho U_\infty^2 HL} \tag{1}$$

$$C_L = \frac{F_L}{1/2\rho U_\infty^2 BL} \tag{2}$$

$$C_M = \frac{M}{1/2\rho U_\infty^2 B^2 L} \tag{3}$$

Aerodynamic coefficients, including the drag force coefficient $C_{D(t)}$, lift force coefficient $C_{L(t)}$, and pitching moment coefficient $C_{M(t)}$, can be obtained with Eqs. (1), (2), and (3), where F_D, F_L, and M are the drag force, lift force, and pitching moment acting on the model in the body axis system (Fig. 5), respectively, which can be measured by the force six-component balances; U_∞ is the test wind speed; L is the length of model; B is the width of model; ρ is the air density; H is the height of model. When calculating the train aerodynamic coefficient, H is assumed equal to the height of the train. In terms of the calculation of the aerodynamic coefficients of bridge deck, H is the sum of the heights of deck and barrier. The pitching moment, M, is calculated with respect to the sectional centroid of the model. For the wind-train-bridge coupling vibration analysis, aerodynamic coefficients are generally used to determine the wind-induced load of train and bridge deck at different wind velocities (Li *et al*. 2005, Li *et al*. 2013, Zhang *et al*. 2018). However, for train-bridge systems, especially those with wind barriers, the complex turbulent field behind the wind barriers makes the measured force unsteady in the wind tunnel. Considering the complexity of unsteady analysis, a unitary value for the admittance function of both the bridge deck and the train has been assumed in this study.

2.3 Wind tunnel test results

According to the time history of force coefficients, the mean coefficients can be obtained by time-averaged. In wind tunnel test, the study focuses not only on the aerodynamic loading of trains, but also on the aerodynamic loading of bridge decks. The recorded experimental results are presented to analyse the influence of wind barriers on

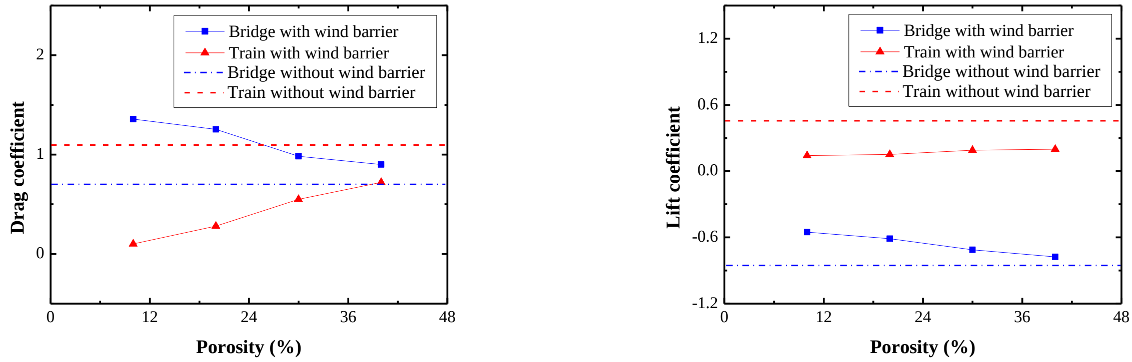

(a) Drag coefficient (b) Lift coefficient

Fig. 6 Effect of wind barrier's porosity on aerodynamic force coefficients of the train-bridge system in windward cases

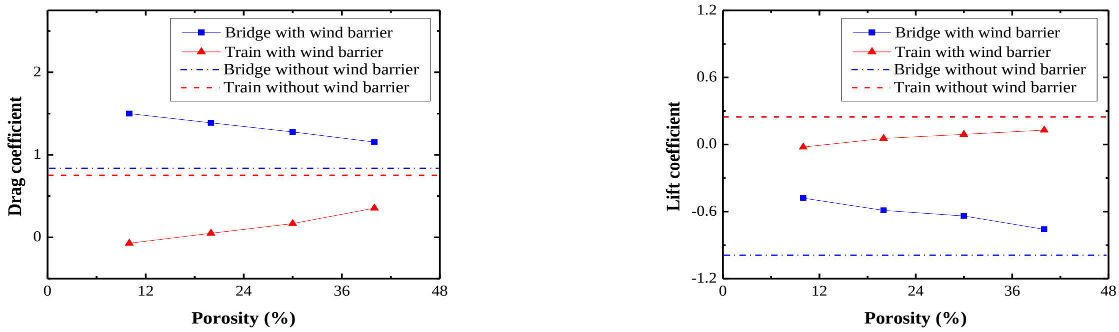

(a) Drag coefficient (b) Lift coefficient

Fig. 7 Effect of wind barrier's porosity on aerodynamic force coefficients of the train-bridge system in leeward cases

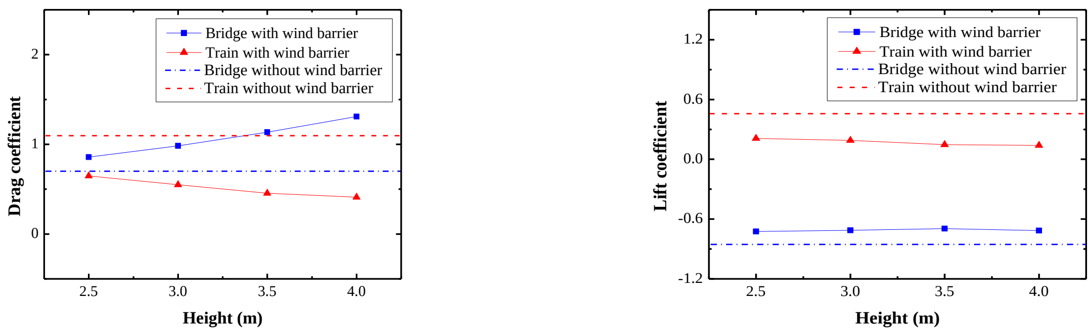

(a) Drag coefficient (b) Lift coefficient

Fig. 8 Effect of wind barrier's height on aerodynamic force coefficients of the train-bridge system in windward cases

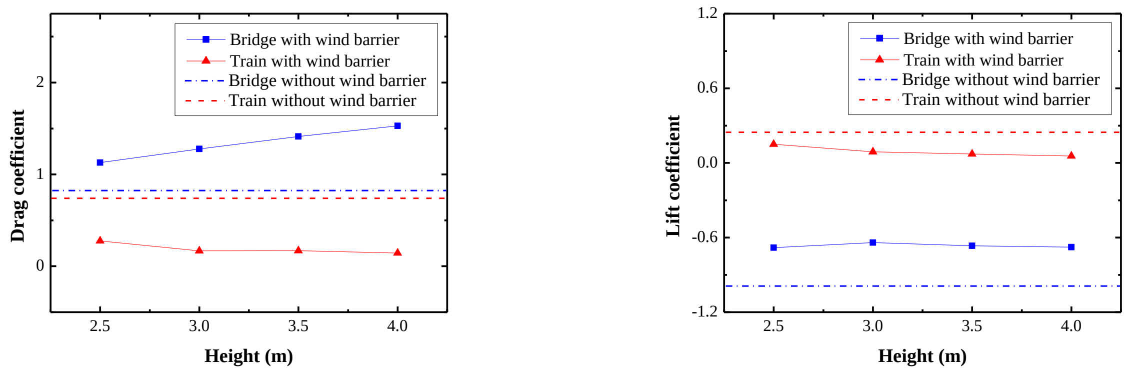

(a) Drag coefficient (b) Lift coefficient

Fig. 9 Effect of wind barrier's height on aerodynamic force coefficients of the train-bridge system in leeward cases

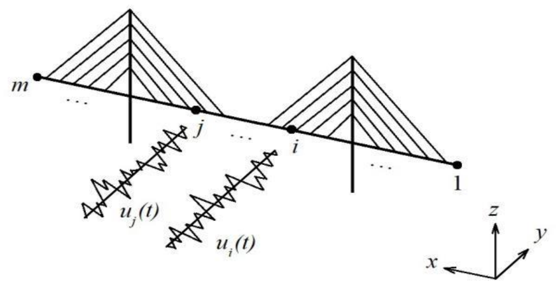

Fig. 10 Spanwise turbulent wind velocities components of the bridge

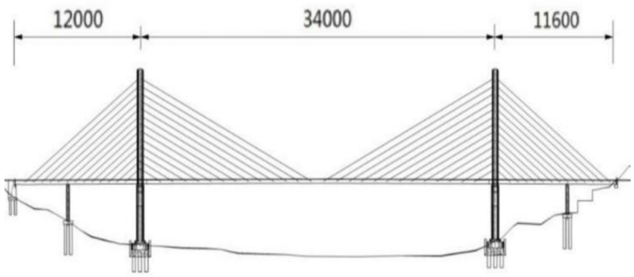

Fig. 11 General information of the bridge (Unit: cm)

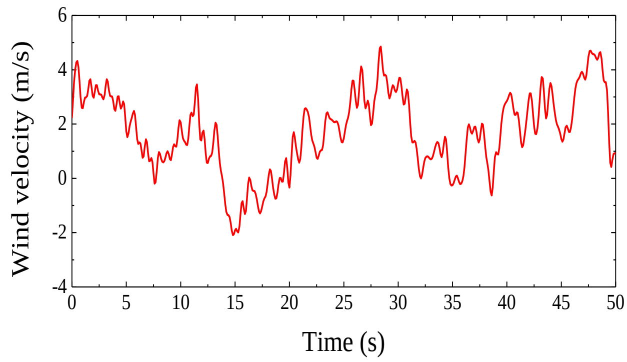

Fig. 12 Time histories of the turbulent horizontal component at mid-span of bridge deck

the aerodynamic forces of the bridge and the train, as shown in Figs. 6, 7, 8 and 9.

By comparing the aerodynamic coefficients of the cases with and without wind barrier, it can be seen that the wind barrier reduces the wind-induced load on the train while bringing more wind-induced load to the bridge deck. The degree of this effect varies depending on the height and porosity of the wind barrier. Figs. 6 and 7 illustrate the change of aerodynamic coefficients with the wind barrier's porosity from 10% to 40% when the wind barrier's height is 3.0 m. As the responses of the bridge and the train depend on the magnitude of the aerodynamic coefficients, this paper compares the absolute values of the data. As shown in Fig. 6, with the increase of the wind barrier's porosity from 10% to 40%, C_D of the bridge decrease by 35% and C_L of the bridge decrease by 41%. On the contrary, with the increased porosity C_D of the train increase by 621% and C_L of the train increase by 54%. Fig. 7 shows the effect of wind barrier's porosity on C_D and C_L of the bridge and the train when the train runs on the leeward lane. The aerodynamic coefficients of windward cases and leeward cases have the same variation tendency. Nevertheless, it can be seen that the wind barrier's porosity has more effect on the aerodynamic coefficients for both the train and the bridge when the train runs on the windward lane. The reason is that the windproof effect of the wind barrier is related to the distance between the train and the wind barrier (Kwon *et al*. 2011, Cornelis *et al*. 2005). Compared with the leeward condition, when the train is on the windward lane, the train is closer to the wind barrier on the windward side, and the change of the wind barrier porosity has a more significant effect on the wind speed in the vicinity of the wind barrier.

Figs. 8 and 9 show the change of aerodynamic coefficients with wind barrier's height ranging from 2.5 m to 4.0 m when the wind barrier's porosity is 30%. As shown in Figs. 8(a) and 9(a), in the case of windward and leeward, the C_D of the bridge increases by 55% and 37% respectively, and the C_D of the train reduces by 40% and 38% respectively. On the other hand, the effect of the wind barrier's height on the C_L of bridge and train is different, as shown in Figs. 8(b) and 9(b). In thecases of windward and leeward, the C_L of the bridge reduces by 41% and 35% respectively, the C_L of the train increases by 7% and 4% respectively. This indicates that the effects of wind barrier's height on C_D and C_L of the train and C_D of the bridge is more significant than on C_L of bridge as the height varies from 2.5 m to 4.0 m. This is because the change in wind barrier height does not significantly change the wind pressure difference between the above and below surfaces of the bridge deck when the train is on the bridge.

The results of wind tunnel tests indicate that reducing porosity and increasing the height of the wind barrier can effectively reduce the wind-induced load of the train in the crosswind environment, but it will also bring more wind-induced load to the bridge deck. Especially when the wind barrier porosity is reduced from 40% to 10% and the wind barrier height is increased from 2.5 m to 4.0 m, the wind-induced drag force on the bridge deck is increased by 35% and 55% respectively. For urban rail transit special cable-stayed bridge, the wind-induced load acting on the bridge deck can cause large deformation and vibration. This is expected to deteriorate the running safety of the bridge. Therefore, the aerodynamic analysis of wind barriers for urban rail transit special cable-stayed bridge is not enough, it is necessary to study the wind barrier influence mechanism from the perspective of wind-train-bridge coupled vibration analysis.

3. Dynamic model for wind-train-bridge system

3.1 Simulation of turbulent wind field

To simulate the fluctuating wind force acting on the train and bridge, a modified spectral representation method

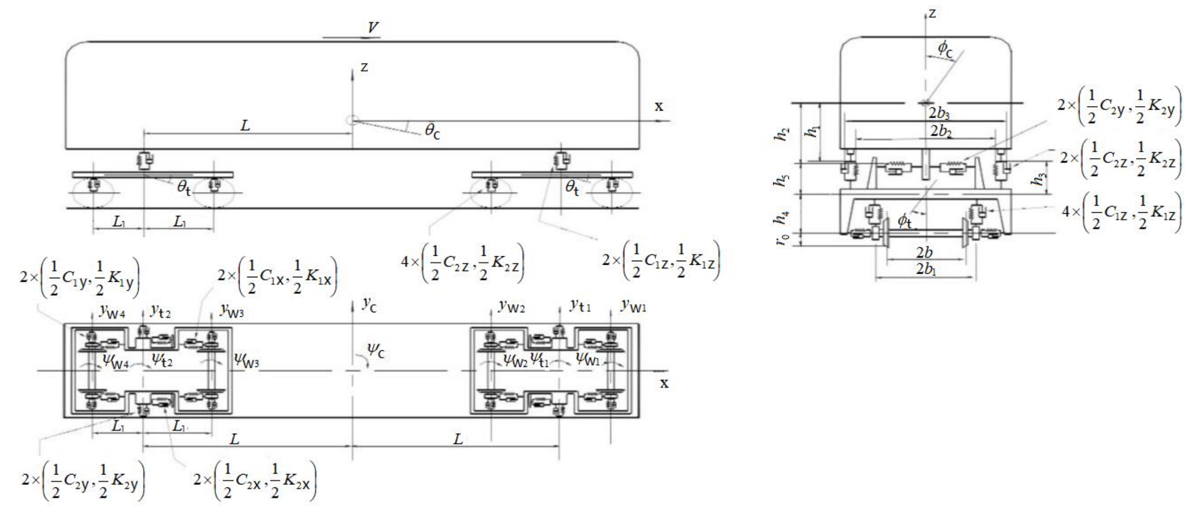

Fig. 13 Mechanical model of the carriage

is used to generate the spanwise turbulence wind field (Scanlan *et al*. 1990, Shinozuka *et al*. 1990). This method is based on the original spectral representation method under the assumption that the wind field is homogeneous along the spanwise direction of the bridge (Yang *et al*. 1997). Considering m wind turbulence processes $u_i(t)$ (i = 1, 2,..., m) of locations along the spanwise direction of a bridge (Fig. 10), and assuming that all the locations are on the same elevation, the spectral density matrix for these m processes can be written as

$$\boldsymbol{S}=\begin{bmatrix} S_{11} & S_{12} & S_{13} & \cdots & S_{1m} \\ S_{21} & S_{22} & S_{23} & \cdots & S_{2m} \\ S_{31} & S_{32} & S_{33} & \cdots & S_{3m} \\ \cdots & \cdots & \cdots & \cdots & \cdots \\ S_{m1} & S_{m2} & S_{m3} & \cdots & S_{mm} \end{bmatrix} \tag{4}$$

According to the previous research (Xu *et al*., 2004), because the bridge is a longitudinal structure along the spanwise direction, only horizontal and vertical fluctuating wind components are considered in simulation of turbulent wind field for bridges.Wind turbulence characteristics of locations along the spanwise direction of the bridge are presented by the Kaimal wind spectrum (Kaimal et al., 1972; Simiu *et al*., 1996). So the horizontal and vertical auto-spectral density functions of the wind turbulence, $u_i(t)$and$w_i(t)$(i = 1, 2,..., m) can be expressed as

$$S_u(n)=\frac{200\, f u_*^2}{n(1+50f)^{5/3}} \tag{5}$$

$$S_w(n)=\frac{3.36\, f u_*^2}{n(1+10f)^{5/3}} \tag{6}$$

where S_u is the auto-spectra of wind turbulence $u_i(t)$,and S_w is the auto-spectra of wind turbulence $w_i(t)$; $f= nz_i/U_i$ is the non-dimensional Monin coordinate; U_i is the mean wind velocity in m/s at altitude z_i; u_* is the shear velocity of the wind flow in m/s; n is the frequency in Hz.

The total length of the bridge is 583 m with a main span of 340 m as shown in Fig. 11. The number of locations for simulating wind velocities is 29. The longitudinal distance between the two adjoin locations is 20 m. The wind speed simulation between adjoin locations is obtained following the Linear Interpolation Algorithm (LIA). In previous studies on the wind-train-bridge coupled vibration analysis (Xu *et al*. 1996, Wang *et al*. 1996), the sampling frequency normally varies in a range from 10Hz to20Hz in simulations of wind field. Besides, the main frequency of the bridge is calculated as 0.4187 Hz. Thus, it is decided to use a sampling frequency of 10 Hz which is broad enough corresponding to the main frequency of the bridge. For a 50 s of sampling duration, the number of computational steps is 500 in total. Typical time-history of the turbulent horizontal component with the mean wind velocity U=25 m/s is shown in Fig. 12.

3.2 Dynamic models for the train and the bridge

The train model consists of eight carriages. Each carriage is composed of seven rigid components, i.e., one body, two bogies, four wheel-sets. As shown in Fig. 13, the bogies are connected with the body and wheel-sets using the spring (K) and damping (C) elements.

To simplify the analysis, it is assumed that the body, bogies, and wheel-sets in each carriage are regarded as rigid components. Each of the body and bogies both has five DOFs (Degrees of freedom): transverse and vertical displacements y, z; rolling ϕ; pitching θ; and yawing Ψ at the centre of gravity. Each wheel-set has two DOFs: transverse displacement y; and yawing Ψ at the center of gravity. In total, a carriage has 23 DOFs.

The case study concerns Gaojiahuayuan Bridge, a streamlined steel-box-girder cable-stayed bridge crossing the Yangtze River in Chongqing, China. The bridge has a main span of 340 m and the height of the tower is 120 m. As a rail transit special cable-stayed bridge, the bridge deck only has two tracks for trains, and the bridge girder adopts a steel box structure. The general information of the bridge is

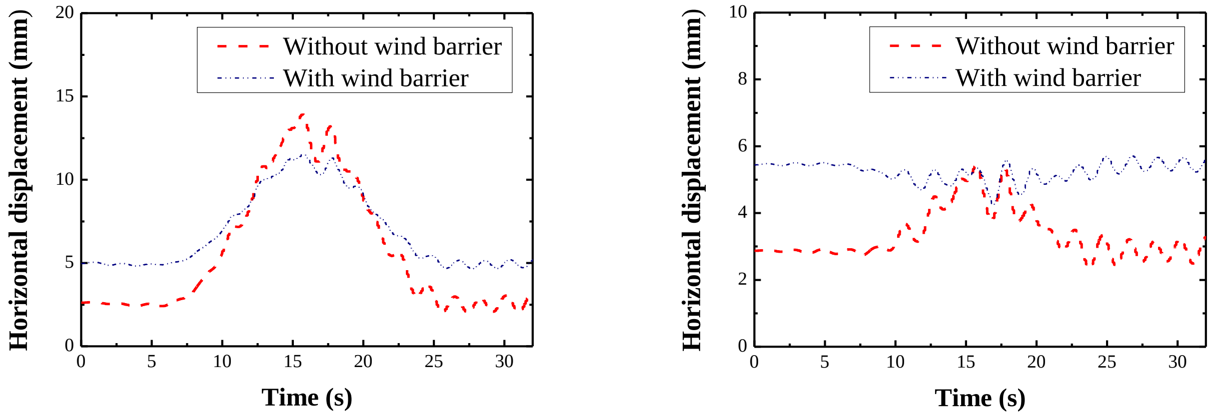

(a) Windward cases (b) Leeward cases

Fig. 14 Time histories of horizontal displacements of the mid-span of the bridge deck

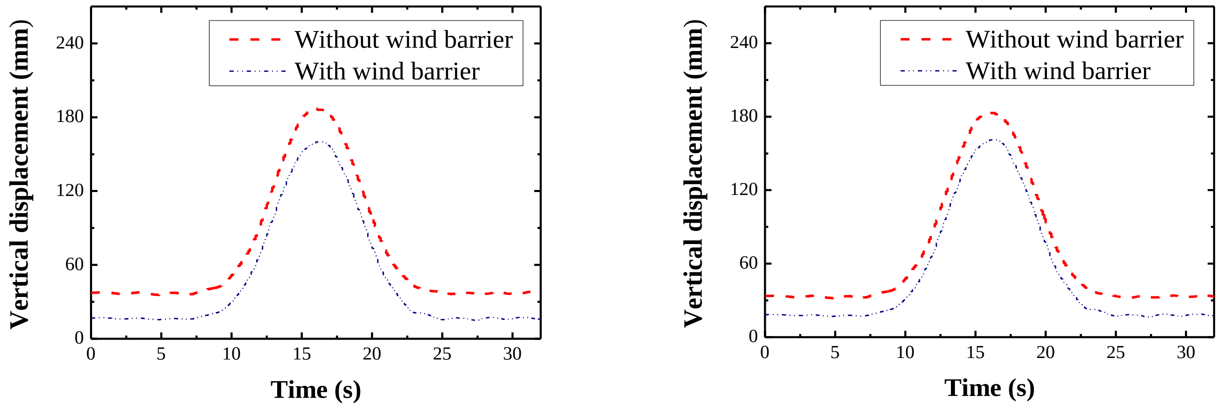

(a) Windward cases (b) Leeward cases

Fig. 15 Time histories of vertical displacements of the mid-span of the bridge deck

shown in Fig. 11.

In this paper, assume that there is no relative movement between the track and bridge deck, a multi-degree of freedom finite element model is adopted. The beam elements are used for bridge girder, tower, and pier. The link element is used for stay cable. The constraint condition between pier and girder is handled by a master-slave node. The girder and the stay-cable are joined by the rigid arm. By adopting this method, a finite element model (FEM) of the bridge is established using a finite element analysis software which was developed by Central South University based on Fortran.

3.3 The space vibration equation of wind-train-bridge system

With D'Alembert's principle applied and the damping force considered, a dynamic problem of an elastic system turns into a problem of dynamic equilibrium. When the train is on the bridge, the total potential energy of the bridge-train elastic dynamic system at time t can be expressed as

$$U_d = U_t + U_b + U_w \tag{7}$$

where U_b is the potential energy of the bridge; U_t is the potential energy of the train; U_w is the potential energy of the wind-induced force.

U_d is only a function of displacements u of an elastic dynamic system at time t. When D'Alembert's principle is applied and the time t is fixed transiently, the dynamic equilibrium of wind-excited bridge-train system with n generalized coordinates requires that is to be

$$\sum_{i=1}^{n} \frac{\partial U_d}{\partial u_i} \delta u_i = 0 \tag{8}$$

Arranging these equations in i =1,2, $\cdots$,n order and writing that in matrix form, one obtains

$$\begin{bmatrix} \boldsymbol{M}_b & \\ & \boldsymbol{M}_t \end{bmatrix} \begin{Bmatrix} \ddot{\boldsymbol{X}}_b \\ \ddot{\boldsymbol{X}}_t \end{Bmatrix} + \begin{bmatrix} \boldsymbol{C}_b + \boldsymbol{C}_{btb} + \boldsymbol{C}_{bw} & \boldsymbol{C}_{bt} \\ \boldsymbol{C}_{tb} & \boldsymbol{C}_t + \boldsymbol{C}_{tt} \end{bmatrix} \begin{Bmatrix} \dot{\boldsymbol{X}}_b \\ \dot{\boldsymbol{X}}_t \end{Bmatrix} + \begin{bmatrix} \boldsymbol{K}_b + \boldsymbol{K}_{btb} + \boldsymbol{K}_{bw} & \boldsymbol{K}_{bt} \\ \boldsymbol{K}_{tb} & \boldsymbol{K}_t + \boldsymbol{K}_{tt} \end{bmatrix} \begin{Bmatrix} \boldsymbol{X}_b \\ \boldsymbol{X}_t \end{Bmatrix} = \begin{Bmatrix} \boldsymbol{P}_{be} + \boldsymbol{P}_{bw} \\ \boldsymbol{P}_{tw} \end{Bmatrix} \tag{9}$$

where $\boldsymbol{M}_b$ and $\boldsymbol{M}_t$ are mass matrixes of the train and the bridge, respectively; $\boldsymbol{C}_b$ and $\boldsymbol{C}_t$ are damping matrixes of the train and the bridge, respectively; $\boldsymbol{C}_{btb}$ and $\boldsymbol{C}_{tb}$ are damping matrixes of train-bridge system caused by the bridge vibration; $\boldsymbol{C}_{bt}$ and $\boldsymbol{C}_{tt}$ are damping matrixes of train-bridge

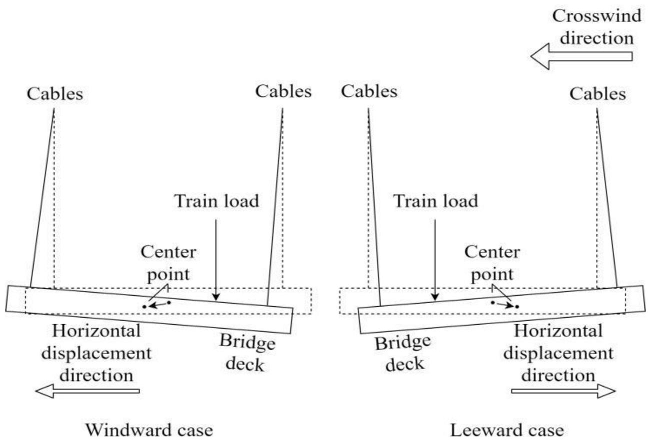

Fig. 16 Schematic diagram of horizontal displacement of bridge deck

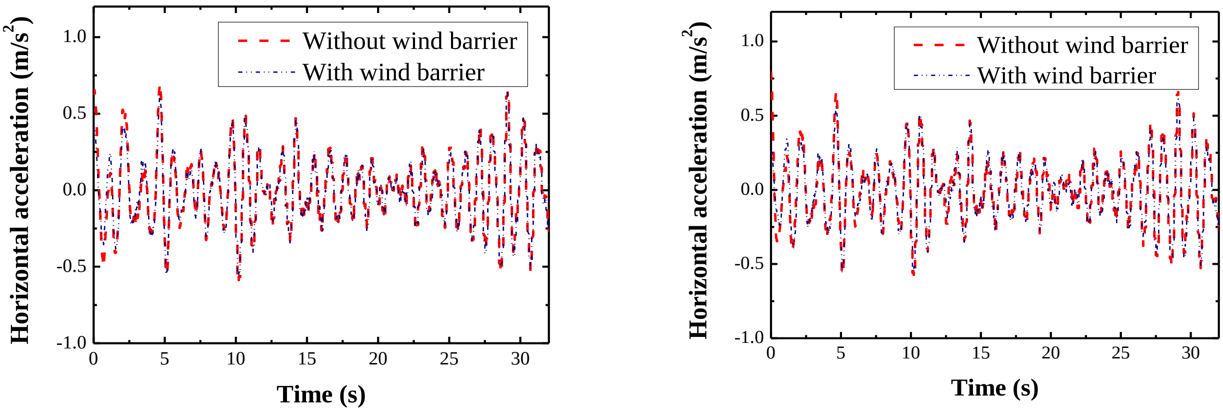

(a) Windward cases (b) Leeward cases

Fig. 17 Time histories of horizontal accelerations of the first carriage

system caused by the train vibration; $\boldsymbol{C}_{bw}$ is damping matrix of bridge caused by the fluctuating wind load; $\boldsymbol{P}_{be}$ is the dead load of train on the bridge; $\boldsymbol{P}_{bw}$ and $\boldsymbol{P}_{tw}$ are the wind load on the train-bridge system; $\boldsymbol{K}$ is stiffness matrix of train-bridge system, the meaning of the subscript is similar to that of the damping matrix. As the second-order linear non-homogeneous differential equation with time-varying coefficients, Eq. (9) can be solved using the Wilson-θ implicit integral algorithm

4. Results and discussion

4.1 Analysis of the time history of dynamic response

In order to study the influence of wind barriers on the time history of dynamic responses of bridge and trains, the dynamic response time history under two conditions, including with and without wind barriers, was analyzed respectively. The calculation was processed under the following conditions: the wind speed at 30 m/s, and the train speed at 80 km/h. Moreover, the porosity of the wind barrier is 30% and the height of the wind barriers is 3.0 m in the calculation. In order to consider the most critical conditions, the train quality needs to be minimal, and the train is in a no-load condition without passengers.

4.1.1 Time history of bridge dynamic response

Fig. 14 and 15 illustrate the time histories of horizontal and vertical displacements of the mid-span of the bridge deck. When the train moves to the mid-span of the bridge, the amplitude of displacement dynamic response curve of the bridge deck at the mid-span increases obviously. By comparing the results of windward and leeward cases, the peak value of the horizontal displacement curve of the bridge deck at the mid-span is larger when the train runs on the windward side of the bridge deck. This is because that on the one hand, as the train moves on either the windward track or the leeward track, the train-induced load produces not only a downward displacement but also a rotation around the center of the cross-section. This rotation may induce a horizontal displacement of the bridge deck. Geometrically, the rotation-related horizontal displacement is in the same direction as the crosswind in terms of the windward cases, whereas the direction is opposite to the crosswind in the leeward cases, as shown in Fig. 16. And on the other hand, the train in the windward cases bear a greater wind-induced load which is transmitted to the bridge deck through the track. Moreover, the effect of the wind barrier on the dynamic response of the bridge deck

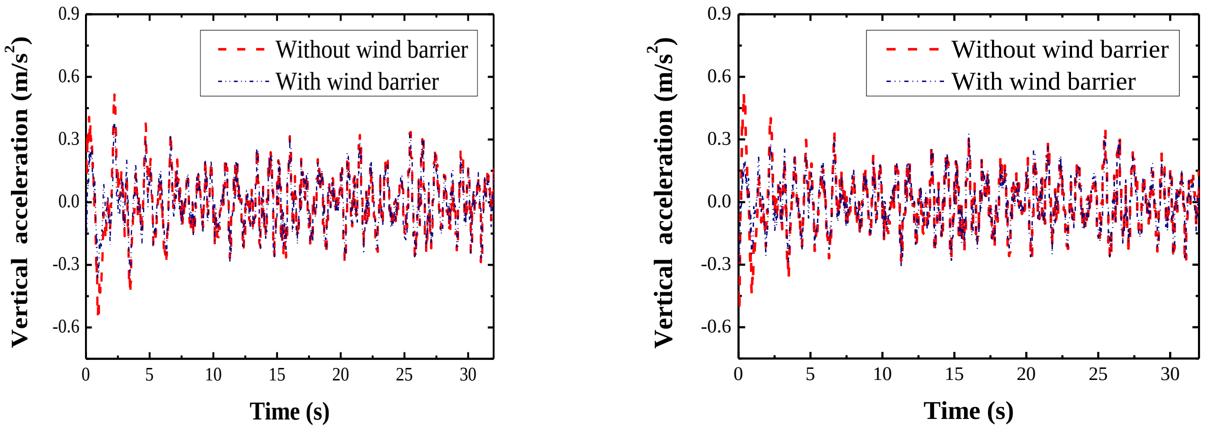

(a) Windward cases (b) Leeward cases

Fig. 18 Time histories of vertical accelerations of the first carriage

Table 1 Description of calculation cases

Case number	Wind speed (m/s)	Height of wind barrier (m)	Porosity of wind barrier (%)
1~4	20	2.5	10, 20, 30, 40
5~8	20	3.0	10, 20, 30, 40
9~12	20	3.5	10, 20, 30, 40
13~16	20	4.0	10, 20, 30, 40
17~20	25	2.5	10, 20, 30, 40
21~24	25	3.0	10, 20, 30, 40
25~28	25	3.5	10, 20, 30, 40
29~32	25	4.0	10, 20, 30, 40
33~36	30	2.5	10, 20, 30, 40
37~40	30	3.0	10, 20, 30, 40
41~44	30	3.5	10, 20, 30, 40
45~48	30	4.0	10, 20, 30, 40
49~52	35	2.5	10, 20, 30, 40
53~56	35	3.0	10, 20, 30, 40
57~60	35	3.5	10, 20, 30, 40
61~64	35	4.0	10, 20, 30, 40

displacement is obvious. As shown in Fig. 14(a), after the wind barrier is set on the bridge deck, the maximum horizontal displacement of the bridge deck at the mid-span reduces by 37%. Compared with the bridge deck equipped with wind barriers, the peak value of the displacement curve of the bridge deck at the mid-span is larger when there is no wind barrier on the bridge deck according to Figs. 14 and 15. The reason is that the wind barrier reduces the influence of the train on the dynamic response of the bridge deck in the crosswind environment. When the train travels to the mid-span of the bridge, the dynamic response of the mid-span bridge deck is mainly affected by the train. After the installation of the wind barrier, the wind-induced load on the train is significantly reduced. The calculation results of wind-train-bridge coupled vibration show that, although the wind barrier brings wind-induced loads to the bridge girder, considering the reduced wind-induced load of the train, the maximum displacement of the bridge deck with the wind barrier is smaller than that without the wind barrier.

4.1.2 Time history of train dynamic response

Figs. 17 and 18 show the time histories of horizontal acceleration responses of the first carriage under the influence of the wind barrier when the train runs on the windward side and the leeward side of the bridge. It can be seen that the influence of the wind barrier on the acceleration time history of the carriage is mainly reflected in the time period when the carriage is running on the first side span of the bridge. The reason is that the wind-induced load of the train has a sharp change at the beginning of the train running on the bridge. In the simulation of the wind-train-bridge coupled vibration, the bridge is in a spanwise strong wind field. This is also in line with the actual situation, because the urban rail transit train is surrounded by buildings before it enters the bridge, and is almost in a windless environment. Thus, the wind environment of the urban rail transit train changes from almost windless to strong at the moment of it moves onto the bridge deck. Fortunately, the wind barrier can effectively reduce the wind-induced load on the train at the initial stage of the train running on the bridge. Moreover, the time history of carriage dynamic response indicates that setting up the wind barrier on the bridge deck can effectively reduce the peak value of the horizontal and vertical acceleration of the carriage when the train runs across the bridge under strong crosswind. When the mean wind speed is 30 m/s in the case of windward and leeward, the wind barrier reduces 13% and 4% of the peak value of the horizontal acceleration of the carriage respectively and reduces 32% and 29% of the peak value of the vertical acceleration of the carriage respectively. Compared with the train running on the windward side of the bridge deck, the peak value of the horizontal and vertical acceleration of the carriage is obviously smaller when the train is running on the leeward side of the bridge deck.

4.2 Analysis of the maximum dynamic response of train

Previous findings indicate that when the train is running

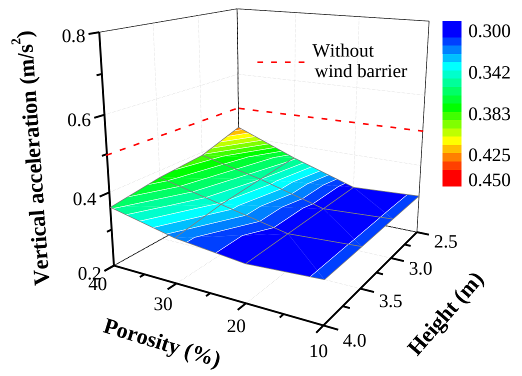

(a) The mean lateral wind speed is 20 m/s

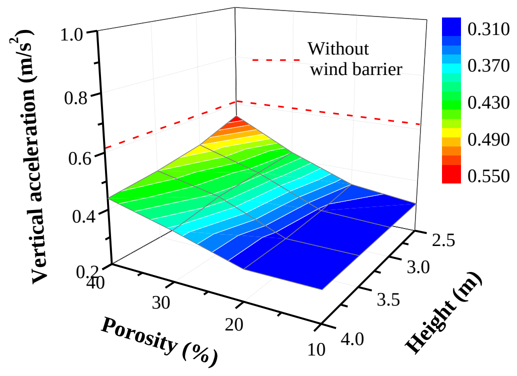

(b) The mean lateral wind speed is 25 m/s

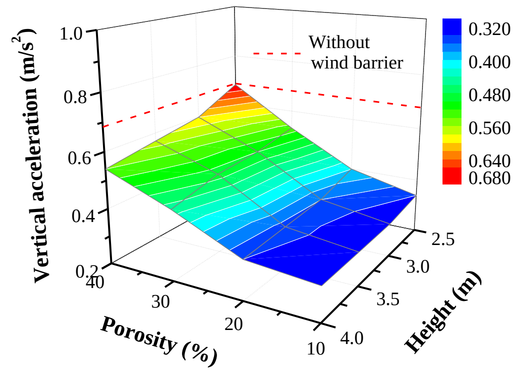

(c) The mean lateral wind speed is 30 m/s

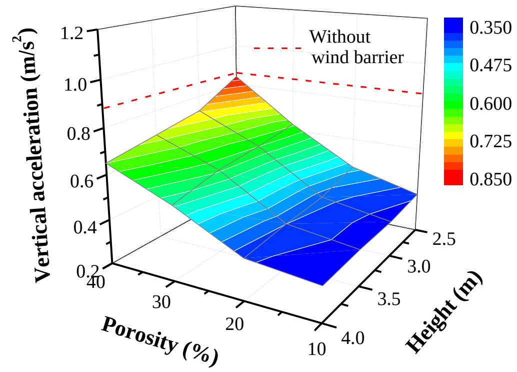

(d) The mean lateral wind speed is 35 m/s

Fig. 20 Maximum vertical accelerations of the train with different heights and porosities wind barriers under the application of crosswind

on the windward side of the bridge, the dynamic response of the train is greater than that on the leeward side of the bridge. Accordingly, the influence of the wind barrier on the train dynamic response is studied only when the train is running on the windward side of the bridge in the following study.

According to previous studies, the main factors influencing the windbreak performance of wind barriers are their porosity and height. Considering the mean wind speeds in the range of 20-35 m/s, the train safety index is calculated under different height and porosity wind barriers to study the influence mechanism of wind barrier's porosity and height on the running safety of urban rail transit cable-stayed bridge. In light of the working conditions arranged as in Table 1, this paper works out the train-bridge dynamic response with a total of 64 cases under the application of crosswind. The calculation of all 64 cases is processed under the following conditions: the deck wind speed from 20 m/s to 35 m/s, the train speed at 80 km/h, wind barrier's porosity from 10% to 40%, and wind barrier's height from 2.5 m to 4.0 m.

4.2.1 Maximum accelerations of the train

Fig. 19 shows the maximum horizontal accelerations of the train when the strain runs through the bridge equipped with different heights and porosities of wind barriers under the attack of crosswind. It can be seen that when the mean lateral wind speed is 20 m/s, the change of wind barrier height and porosity has very little influence on the maximum horizontal acceleration of the train. However, when the mean lateral wind speed is greater than 25 m/s, the maximum horizontal acceleration of the train is apparently influenced by the change of the wind barrier's height and the change of the wind barrier's porosity. It also can be seen that when the mean lateral wind speed is less than 25 m/s, the horizontal acceleration of the train increases slightly with the decrease of wind barrier porosity. This is because the decrease of porosity of the wind barrier increases the lateral wind load of the bridge deck in the crosswind. Under the condition of low lateral wind speed, the influence of the bridge on the horizontal dynamic response of train is greater than that of wind load on train horizontal dynamic response. With the increase of wind barrier's porosity and the decrease of the wind barrier's height, the maximum horizontal acceleration of the train increases significantly. When wind barrier is set with 40% porosity and 2.5 m height, the maximum horizontal acceleration of the train is close to the case without wind barrier. It can also be observed that when the porosity of the wind barrier is less than 20%, the horizontal acceleration of the train does not change obviously with the height of the wind barrier increasing from 2.5 m to4.0 m.

Fig. 20 illustrates a comparison of the maximum vertical accelerations of the train when the train runs through the bridge equipped with different heights and porosities wind barriers under the attack of crosswind. It can be seen that

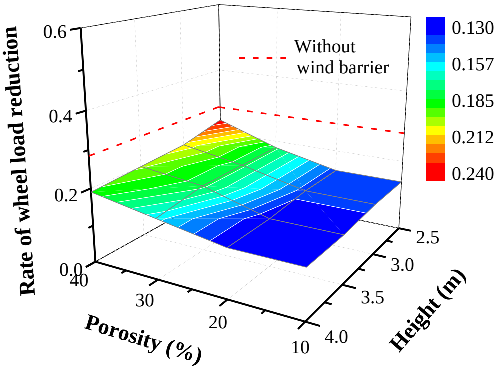

(a) The mean lateral wind speed is 20 m/s

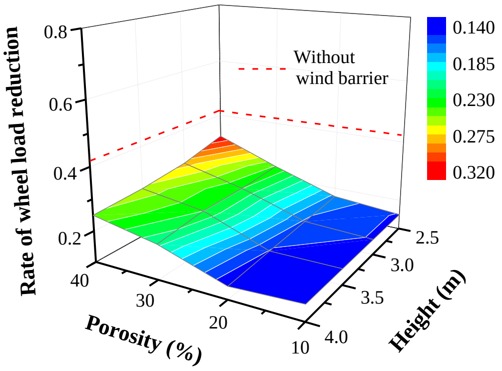

(b) The mean lateral wind speed is 25 m/s

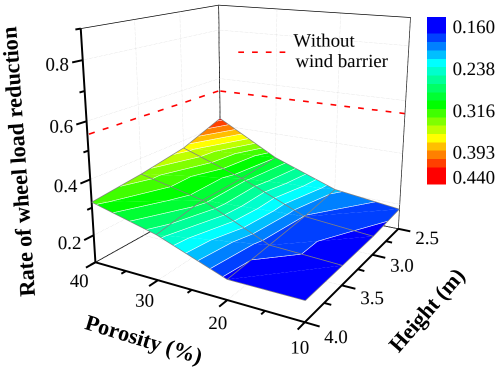

(c) The mean lateral wind speed is 30 m/s

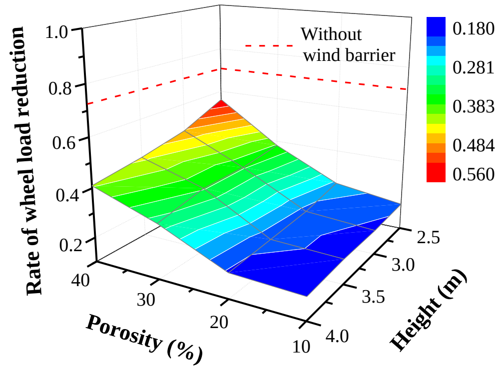

(d) The mean lateral wind speed is 35 m/s

Fig. 21 Rate of wheel load reduction of the train with different heights and porosities wind barriers under the application of crosswind

4.2.2 Rate of wheel load reduction

Wheel load reduction refers to a phenomenon that the wheel weight is lower under the action of a dynamic load than that under the action of the static load. The rate of wheel load reduction is the ratio of wheel load reduction to the average load of the left and right wheels. It can be obtained with Eq. (10), where P_1 and P_2 are left and right wheel weights respectively, and ΔP is the wheel load reduction, and $\bar{P}$ is the average load of the left and right wheels.

$$\begin{cases} \bar{P} = \dfrac{1}{2}\left(P_1 + P_2\right) \\ \Delta P = \dfrac{1}{2}\left(P_2 - P_1\right) \end{cases} \tag{10}$$

Fig. 21 presents a comparison of the maximum rate of wheel load reduction of the rail transit trains after installing wind barriers with different heights and porosities. The rate of wheel load reduction of the train decreases obviously after installing wind barriers. As shown in Fig. 21, in the case of high wind speed, the change of the height and porosity of the wind barrier has a more obvious influence on the maximum rate of wheel load reduction of the train. On the other hand, compared with the increase of the height of the wind barrier, the decrease of the wind porosity of the barrier can effectively control the maximum value of the rate of wheel load reduction when the train is crossing the bridge. When wind barrier porosity reduced from 40% to 20%, the decrease in the maximum rate of wheel load reduction of the train is particularly obvious.

4.2.3 Derailment coefficient

The derailment coefficient is the key index to evaluate the running stability of the train. The derailment coefficient is defined as the ratio (Q/P) of the lateral pressure of the wheel (Q) to the weight of the wheel (P). In this study, the derailment coefficient can be obtained directly according to the physical meaning with the results of the lateral pressure of the wheel and the weight of the wheel from dynamic analysis.

Fig. 22 illustrates the effect of the wind barrier's height and porosity on the maximum derailment coefficients of the rail transit train. It can be seen that the wind barrier can effectively reduce the derailment coefficient, especially in strong crosswind with wind speed higher than 30m/s. The maximum derailment coefficients of the rail transit train reduce with the decrease of wind barrier's porosity and the increase of wind barrier's height. It can also be observed that the influence of the change of porosity on the derailment coefficients of the rail transit train is much greater than that of the change of the height of the wind barrier. The results indicate that when the wind barrier's porosity is40% and the wind barrier's height is less than 3.0 m, the maximum derailment coefficients of the rail transit

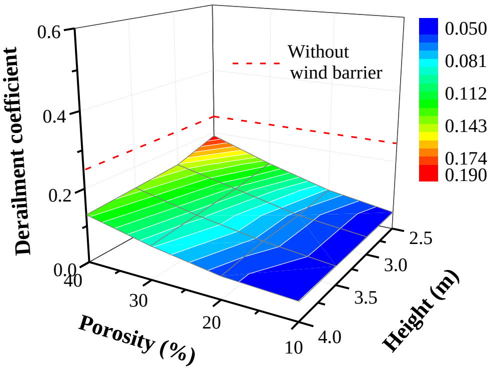

(a) The mean lateral wind speed is 20 m/s

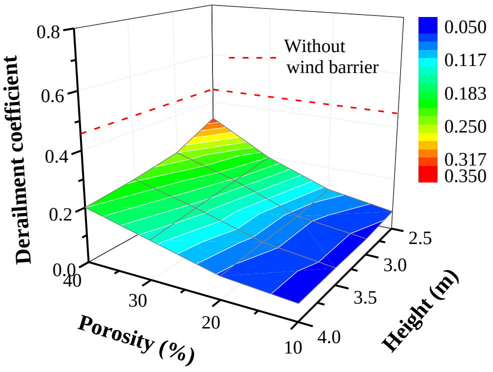

(b) The mean lateral wind speed is 25 m/s

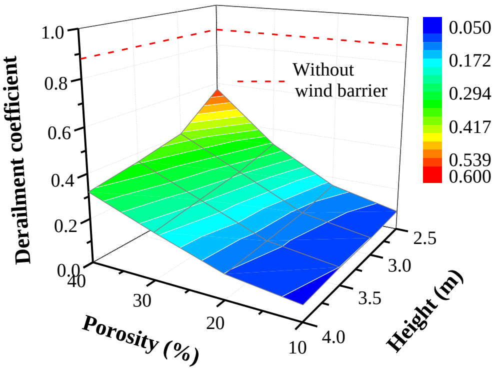

(c) The mean lateral wind speed is 30 m/s

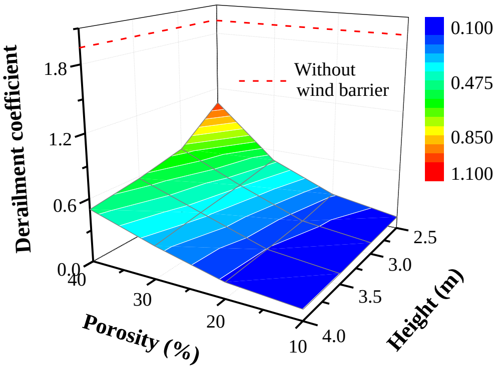

(d) The mean lateral wind speed is 35 m/s

Fig. 22 Derailment coefficient of the train with different heights and porosities wind barriers under the application of crosswind

train does not meet the requirement of train running safety in the case of high lateral wind speed.

5. Conclusions

Taking the first urban rail transit cable-stayed bridge of China as the engineering background, this paper studies the mechanism of the effect of wind barrier on the running safety of trains from the perspective of aerodynamic analysis and wind-train-bridge coupled vibration analysis. Because the urban rail transit cable-stayed bridge tends to be more vulnerable to wind due to its relatively low stiffness and lightweight, the aerodynamic analysis considered the combined effects of wind barriers on the aerodynamic characteristics of the bridge deck and trains. The measurement method in this study is improved to obtain the aerodynamic force of the section model of the bridge deck and trains concurrently in a wind tunnel. Moreover, the aerodynamic coefficients of the bridge deck and trains from the wind tunnel tests are adopted to realize the simulation of the wind-induced load of the train-bridge system. Furthermore, this study reveals the interdependent relationship between porosity and height of wind barrier on the urban rail transit cable-stayed bridge through the wind-train-bridge coupled vibration analysis. Based on the analytical results of the bridge and trains for the bridge equipped with wind barriers of different characteristics, the major conclusions are summarized as follows.

• The results of wind tunnel tests indicate that, for the urban rail transit cable-stayed bridge, the extent of the wind barrier effect on the wind-induced load of the train and bridge deck is different from other types of bridges and trains. Specifically, as the wind barrier porosity is reduced from 40% to 10% and the wind barrier height is increased from 2.5 m to 4.0 m, the wind-induced drag force on the bridge deck is increased by 35% and 55% respectively. These additional large forces may induce unexpected vibrations especially for structural types with relatively low rigidity and mass. Thus, reducing porosity and increasing height of the wind barrier are not always the best choice for the targeted urban rail transit cable-stayed bridges.

• Even though more wind forces acting on the bridge are caused by the setting of wind barriers, it is found that the displacement dynamic response of the bridge deck decreases obviously when the train runs through the bridge after the wind barrier is set on the urban rail transit special cable-stayed bridge deck. This indicates that setting the wind barrier on the bridge deck can effectively reduce the dynamic responses of both the trains and bridge, which is a favorable phenomenon attributed to the wind barriers. The influence of the wind barrier on the acceleration time history of the carriage is mainly observed in the time period when the train is running on the first side span of the bridge.

• In comparison with the increase of the height of the wind barrier, the decrease of the porosity of the wind barrier can effectively control the maximum value of the derailment coefficient and rate of wheel load reduction when the train is crossing the urban rail transit cable-stayed bridge. This is because, compared to the change in height, the change of the wind barrier porosity has a greater influence on the train's aerodynamic coefficient as observed in the wind tunnel tests.

Based on the obtained results, the wind barrier is recommended to be set with 20% porosity and 2.5 m height for the urban rail transit cable-stayed bridge when the train crosses it under the crosswind of 35 m/s mean wind speed. This conclusion can provide a reference for the wind barrier setting on the other urban rail transit cable-stayed bridge.

Acknowledgments

The research results of this paper are supported in part by the National Key R&D Program of China (2017YFB1201204). The work is also sponsored by the National Nature Science Foundation of China (51378511,51678576) and the Provincial Natural Science Research Project of Anhui Province (KJ2019A0744). The authors are also very grateful to the staff in the National Engineering Laboratory for High-Speed Railway Construction at Central South University.

References

Baltaxe, R. (1967), “Air flow patterns in the lee of model windbreaks”, *Theor. Appl. Climatol.*, **15**(3), 287-312. https://doi.org/10.1007/BF02243857.

Buljac, A., Kozmar, H., Pospíšil, S. and Macháček, M. (2017), “Aerodynamic and aeroelastic characteristics of typical bridge decks equipped with wind barriers at the windward bridge-deck edge”, *Eng. Struct.*, **137**(15), 310-322. https://doi.org/10.1016/j.engstruct.2017.01.055.

Charuvisit, S., Kimura, K. and Fujino, Y. (2004),“Effects of wind barrier on a vehicle passing in the wake of a bridge tower in cross wind and its response”, *J. Wind Eng. Indus. Aerod.*, **92**(7), 609-639. https://doi.org/10.1016/j.jweia.2004.03.006.

Chen, N., Li, Y.L. and Wang, B. (2015), “Effects of wind barrier on the safety of vehicles driven on bridges”, *J. Wind Eng. Indus. Aerod.*, **143**, 113-127. https://doi.org/10.1016/j.jweia.2015.04.021.

Chu, C.R., Chang, C.Y., Huang, C.J., Wu, T.R., Wang, C.Y., Liu, M.Y., Cornelis, W.M. and Gabriels, D. (2013), “Windbreak protection for road vehicles against crosswind”, *J. Wind Eng. Indus. Aerod.*, **116**, 61-69. https://doi.org/10.1016/j.jweia.2013.02.001.

Cornelis, W.M. and Gabriels, D. (2005), “Optimal windbreak design for wind-erosion control”, *J. Arid Environ.*, **61**(2), 315-332. https://doi.org/10.1016/j.jaridenv.2004.10.005.

Dong, Z., Luo, W., Qian, G. and Wang, H. (2007), “A wind tunnel simulation of the mean velocity fields behind upright porous fences”, *Agr. Forest Meteorol.*, **146**, 82-93. https://doi.org/10.1016/j.agrformet.2007.05.009.

Dorigatti, F., Sterling, M., Rocchi, D., Belloli, M., Quinn, A.D., Baker, C.J. and Ozkan, E. (2012),“Wind tunnel measurements of crosswind loads on high sided vehicles over long span bridges”, *J. Wind Eng. Indus. Aerod.*, **107-108**, 214-224. https://doi.org/10.1016/j.jweia.2012.04.017.

Gandemer, J. (1981), “The aerodynamic characteristics of windbreaks, resulting in empirical design rules”, *J. Wind Eng. Indus. Aerod.*, **7**, 15-36. https://doi.org/10.1016/0167-6105(81)90065-9.

Guo, W.W., Wang, Y.J., Xia, H. and Lu, S. (2015), “Wind tunnel test on aerodynamic effect of wind barriers on train-bridge system”, *Sci. China Technol. Sc.*, **58**(2), 219-225. https://doi.org/10.1007/s11431-014-5675-1.

Han, Y., Cai, C.S., Zhang, J.R., Chen, S.R. and Xia, H. (2014), “Effects of aerodynamic parameters on the dynamic responses of road vehicles and bridges under cross winds”, *J. Wind Eng. Indus. Aerod.*, **134**, 78-95. https://doi.org/10.1016/j.jweia.2014.08.013.

Han, Y., Hu, J., Cai, CS., Chen, Z. and Li C. (2013), “Experimental and numerical studies of aerodynamic forces on vehicles and bridges”, *Wind Struct.*, **17**(2), 163-184. https://doi.org/10.12989/was.2013.17.2.163.

He, X.H., Shi, K., Wu, T., Zou, Y.F., Wang, H.F. and Qin, H.X. (2016), “Aerodynamic performance of a novel wind barrier for train-bridge system”, *Wind Struct.*, **23**(3), 2-20. https://doi.org/10.12989/was.2016.23.3.171.

Heisler, G.M. and Dewalle, D.R. (1988), “Effects of windbreak structure on wind flow”, *Agric. Ecosyst. Environ.*, **22-23**, 41-69. https://doi.org/10.1016/0167-8809(88)90007-2.

Jeffries, W.Q., Infield, D.G. and Manwell, J. (1991), “Limitations and recommendations regarding the Shinozuka method for simulating wind data”, *Wind Eng.*, **15**(3), 147-154. https://www.jstor.org/stable/43749452.

Judd, M.J., Raupach, M.R. and Finnigan, J.J. (1996), “A wind tunnel study of turbulent flow around single and multiple windbreaks, Part I: velocity fields”, *Bound. Layer Meteorol.*, **80**, 127-165. https://doi.org/10.1007/BF00119015.

Kaimal, J.C., Wyngaard, J.C., Izumi, Y. and Cote, O.R. (1972), “Spectral characteristics of surface-layer turbulence”, *Quart. J. R. Met. Soc.*, **98**, 563-589. https://doi.org/10.1002/qj.49709841707.

Kozmar, H., Procino, L., Borsani, A. and Bartoli, G. (2012), “Sheltering efficiency of wind barriers on bridges”, *J. Wind Eng. Indus. Aerod.*, **107-108**, 274-284. https://doi.org/10.1016/j.jweia.2012.04.027.

Kozmar, H., Procino, L., Borsani, A. and Bartoli, G. (2014), “Optimizing height and porosity of roadway wind barriers for viaducts and bridges”, *Eng Struct.*, **81**, 49-61. https://doi.org/10.1016/j.engstruct.2014.09.029.

Kwon, S.D., Kim, D.H., Lee, S.H. and Song, H.S. (2011), “Design criteria of wind barriers fortraffic Part1: wind barrier performance”, *Wind Struct.*, **14**(1), 55-70. https://doi.org/10.12989/was.2011.14.1.055.

Larsen, A. and Walther, J.H. (1998), “Discrete vortex simulation of flow around five generic bridge deck sections”, *J. Wind Eng. Indus. Aerod.*, **77-78**, 591-602. https://doi.org/10.1016/S0167-6105(98)00175-5.

Lee, S.J. and Kim, H.B. (1998), “Velocity field measurements of flow around a triangular prism behind a porous fence”, *J. Wind Eng. Indus. Aerod.*, **77-78**, 521-530. https://doi.org/10.1016/S0167-6105(98)00169-X.

Lee, S.J. and Kim, H.B. (1999), “Laboratory measurements of velocity and turbulence field behind porous fences”, *J. Wind Eng. Indus. Aerod.*, **80**, 311-326. https://doi.org/10.1016/S0167-6105(98)00193-7.

Li, Y., Qiang, S., Liao, H. and Xu, Y.L. (2005), “Dynamics of wind-rail vehicle-bridge systems”, *J. Wind Eng. Indus. Aerod.*, **93**(6), 483-507. https://doi.org/10.1016/j.jweia.2005.04.001.

Li, Y.L., Liao, H.L. and Qiang, S.Z. (2004), “Study on aerodynamic characteristics of the vehicle-bridge system by the section model wind tunnel test", *J. China Railw. Soc.*, **3**, 71-75. https://doi:10.3321/j.issn:1001-8360.2004.03.014.

Li, Y.L., Xiang, H.Y., Wang, B., Xu, Y.L. and Qiang, S.Z. (2013), "Dynamic analysis of wind-vehicle-bridge coupling system during the meeting of two trains", *Adv. Struct. Eng.*, **16**(10), 1663-1670. https://doi.org/10.1260/1369-4332.16.10.1663.

Matsuda K., Cooper K.R., Tanaka H. Tokushige, M. and Iwasaki T. (2001), "An investigation of Reynolds number effects on the steady and unsteady aerodynamic forces on a 1:10 scale bridge deck section model", *J. Wind Eng. Ind. Aerod.*, **89**, 619-632. https://doi.org/10.1016/S0167-6105(01)00062-9.

Santiago, J.L., Martin, F., Cuerva, A., Bezdenejnykh, N. and Sanz-Andres, A., (2007), "Experimenal and numerical study of wind flow behind windbreaks", *Atmos. Environ.*, **41**, 6406-6420. https://doi.org/10.1016/j.atmosenv.2007.01.014.

Scanlan, R.H. and Jones, N.P. (1990), "Aeroelastic analysis of cable-stayed bridges", *J. Struct. Eng.*, **116**(2), 279-297. https://doi.org/10.1061/(ASCE)0733-9445(1990)116:2(279).

Schewe, G. and Larsen, A. (1998), "Reynolds number effects in the flow around a bluff bridge deck cross section", *J. Wind Eng. Indus. Aerod*., **74-76**, 829-838. https://doi.org/10.1016/S0167-6105(98)00075-0.

Shinozuka, M., Yun, C.B. and Seya, H. (1990), "Stochastic methods in wind engineering", *J. Wind Eng. Indus. Aerod.*, **36**, 829-843. https://doi.org/10.1016/0167-6105(90)90080-V.

Simiu, E. and Scanlan, R.H. (1996), "Wind Effects on Structures: Fundamentals and Application to Design", John Wiley & Sons, New York, NY, U.S.A.

Simiu. E. and Scanlan. R.H. (1978), *Wind effects on structures*, Wiley, New York, NY, U.S.A.

Su, Y., Xiang, H.Y., Fang, C., Wang, L. and Li, Y.L. (2017), "Wind tunnel tests on flow fields of full-scale railway wind barriers", *Wind Struct.*, **24**(2), 171-184. https://doi.org/10.12989/was.2017.24.2.171.

Wang, S.Q., Xia, H., Guo, W.W. and Zhang, N. (2010), "Nonlinear dynamic response analysis of a long-span suspension bridge under running train and turbulent wind", *Interact. Multiscale Mech.*, **3**(4), 309-320. https://doi.org/10.12989/IMM.2010.3.4.309.

Wu, X.X., Zou, X.Y. and Zhang, C.L. (2013), "The effect of wind barriers on airflow in a wind tunnel", *J. Arid. Environ.*, **97**, 73-83. https://doi.org/10.1016/j.jaridenv.2013.05.003.

Xiang, H.Y., Li, Y.L. and Wang, B. (2015), "Aerodynamic interaction between static vehicles and wind barriers on railway bridges exposed to crosswinds", *Wind Struct.*, **20**(2), 237-247. https://doi.org/10.12989/was.2015.20.2.237.

Xiang, H.Y., Li, Y.L., Chen, B. and Liao, H.L. (2014), "Protection effect of railway wind barrier on running safety of train under cross winds", *Adv. Struct. Eng.*, **17**(8), 1177-1187. https://doi.org/10.1260/1369-4332.17.8.1177.

Xiang, H.Y., Li, Y.L., Chen, S.R. and Hou, G.Y. (2018), "Wind loads of moving vehicle on bridge with solid wind barrier", *Eng. Struct.*, **156**(1), 188-196. https://doi.org/10.1016/j.engstruct.2017.11.009.

Xu, Y.L. and Guo, W.H. (2003), "Dynamic analysis of coupled road vehicle and cable-stayed bridge systems under turbulent wind", *Eng. Struct.*, **25**(4), 473-486. https://doi.org/10.1016/S0141-0296(02)00188-8.

Xu, Y.L. and Guo, W.H. (2004), "Effects of bridge motion and crosswind on ride comfort of road vehicles", *J. Wind Eng. Ind. Aerodyn.*, **92**(7-8), 641-662. https://doi.org/10.1016/j.jweia.2004.03.009.

Xu, Y.L., Zhang, N. and Xia, H. (2004), "Vibration of coupled train and cable-stayed bridge systems in cross winds", *Eng. Struct.*, **26**(10), 1389-1406. https://doi.org/10.1016/j.engstruct.2004.05.005.

Yang, W.W., Chang, T.Y.P. and Chang, C.C. (1997), "An efficient wind field simulation technique for bridges", *J. Wind Eng. Indus. Aerod.*, **67-68**, 697-708. https://doi.org/10.1016/S0167-6105(97)00111-6.

Zhang, T., Xia, H. and Guo, W.W. (2018), "Analysis on running safety of train on the bridge considering sudden change of wind load caused by wind barriers", *Front. Struct. Civ. Eng.*, **12**(4), 558-567. https://doi.org/10.1007/s11709-017-0455-1.

Zhang, T., Xia, H. and Guo, WW. (2013), "Analysis on running safety of train on bridge with wind barriers subjected to cross wind", *Wind Struct.*, **17**(2), 203-225.https://doi.org/10.12989/was.2013.17.2.203.

FR